Scanning Wavefront Sensor for Measurement of Highly Divergent Optics

Martin E. Fuerst * **Georg Schitter** *

* *Christian Doppler Laboratory for Precision Engineering for Automated In-Line Metrology, Automation and Control Institute, Vienna University of Technology (e-mail: martin.fuerst@tuwien.ac.at)*

Abstract: This paper deals with the characterization of freeform optics by means of a wavefront sensor. Freeform optics show an increasing demand since they have the potential to improve optical system performance while reducing size, weight and complexity. To directly measure the performance of a freeform optical part, a novel scanning wavefront sensor approach is proposed which is faster than a coordinate measuring machine and more flexible than an interferometer. The challenges lie in the limited dynamic range of a Shack-Hartmann sensor concerning wavefront slope and curvature. Both limits can be overcome by repositioning the sensor and orienting it tangentially to the wavefront. An automatic setup is developed and first measurements are demonstrated on a highly divergent wavefront. It is shown that the dynamic range of the sensor is increased by scanning the sensor along the wavefront and orienting the sensor tangential to the wavefront in each position. Measurements are taken over a range of $\pm 15°$, which is an improvement by a factor 5 compared to the typical dynamic range of $\pm 3°$ for a static Shack-Hartmann sensor.

Keywords: Freeform optics, optical metrology, wavefront measurement, scanning system, Shack-Hartmann sensor, surface metrology

1. INTRODUCTION

Freeform optics have a high potential for small packaging size and high optical performance in light distribution and light detection applications. Assefa et al. (2018) demonstrate the potential of freeform optics for energy efficient illumination with LEDs, while Reimers et al. (2017) were able to design a freeform spectrometer that is five times more compact than comparable conventional designs. Current research investigates the potential of freeform optics in the micro scale, e.g. aspheric contact lenses [Li and Fang (2019)] and the macro scale, e.g. telescope mirrors [Graves et al. (2019)]. In the first case, medical benefits are expected, while in the second case, astronomical images of unprecedented quality may be achieved through the reduction of aberrations.

The high-precision manufacturing of freeform parts relies on high-precision metrology [Fang et al. (2013)]. In general, there is a large number of measurement methods for non-optical freeform surfaces such as turbine blades, automotive parts or airplane fuselage: tactile and optical coordinate measuring machines, interferometric and deflectometric techniques, profilometry and laser trackers [Savio et al. (2007)]. However, only few of these techniques are suitable for freeform *optics* because optical parts typically require very fine tolerances ($< 10^{-5}$), are typically medium sized (range of mm to m) and are often transparent [Savio et al. (2007)].

The two main methods to be considered are coordinate measuring machines and interferometric methods: Interferometric techniques offer sub-nm resolution and are thus a well known solution for fast measurement of flats and spheres. Aspheric surfaces can also be measured with interferometric techniques through the use of null-optics (refractive or diffractive). However, this constitutes a huge loss of universality in the measurement tool, as a new surface geometry requires a new null-lens [Kim et al. (2004)]. The fabrication of an application-specific null-lens is costly and also introduces additional uncertainties (alignment, fabrication quality, residual aberrations) to the measurement procedure. Also, interferometric methods are very sensitive to vibrations and thus difficult to use in industrial environments.

Coordinate measuring machines (CMMs) are very flexible and can be equipped with tactile or optical non-contact probes. For optical (possibly coated) parts, non-contact probes are favoured as they do not damage the surface under test. Henselmans et al. (2011) developed a non-contact measurement machine for freeform optics which resembles a giant CD-player and utilizes a probe based on the differential confocal method. Compared to interferometric methods, which are typically "one-shot" measurements, CMMs are relatively slow as they have to acquire surface geometries point by point. For rotationally symmetric parts, this can be mitigated by scanning a single line; for freeform surfaces, the whole geometry has to be scanned, resulting in long measurement times (minutes to hours). Another recent example of an optical, scanning method for freeform surface metrology is reported [Zapico et al. (2018)], using a conoscopic holography sensor for on-machine-measurement of CNC-machined freeform parts.

Post-print version of the article: M. E. Fuerst and G. Schitter, "Scanning Wavefront Sensor for Measurement of Highly Divergent Optics," *IFAC PapersOnLine*52-15 (2019) 25–30, 2019. DOI: 10.1016/j.ifacol.2019.11.644

Fang et al. (2013) point out a second way of freeform part metrology: Instead of measuring the freeform part surface, the freeform part *performance* can be measured. This can be achieved by measuring the optical wavefront that is transmitted or reflected by an optical system, for instance with a Shack-Hartmann sensor. A Shack-Hartmann sensor is a camera-based optical wavefront sensor that allows to measure a region of the wavefront reflected or transmitted by an optical system [Platt and Shack (2001)]. It consists of a lenslet array that segments the incoming wavefront onto an imaging chip, where the positions of the focussed spots are detected. From this spot pattern, the wavefront shape can be reconstructed, as long as the curvature of the incoming wavefront is not large enough to create ambiguities [Rocktäschel and Tiziani (2002)]. Shack-Hartmann sensors are small, robust to vibrations and fast, so they are well suited for application in industrial environments [Thier et al. (2013)]. Their capability to characterize lenses that are bigger than the sensor aperture was recently demonstrated [Burada et al. (2017), Pant et al. (2015)]. This was done by manual, linear repositioning of the sensor and subsequent stitching of the acquired wavefront subaperture images.

The contribution of this paper is to propose an automatic setup that allows for arbitrary repositioning and reorientation of a Shack-Hartmann sensor. As discussed in section 2, this allows the measurement of arbitrary wavefront shapes and is especially useful for highly divergent wavefronts because the wavefront curvature automatically decreases with an increased measurement distance. In combination with a reliable stitching algorithm, a measurement of the complete, global, wavefront exiting a freeform optic allows characterization of the part performance. Compared to an interferometric approach, this technique does not need any null-optics and is less sensitive to environmental vibrations. Compared to a coordinate measuring machine, the Scanning Shack-Hartmann Sensor (SSHS) approach offers higher speed and avoids damaging the part (compared to a tactile CMM). In section 3, an automatic setup is constructed and wavefront measurements on a highly-divergent optic are taken. The device under test for this demonstration is not a freeform optic, but its numerical aperture (NA) exceeds the dynamic range of a static Shack-Hartmann sensor and thus serves to demonstrate the measurement principle. In section 4, it is demonstrated that the dynamic range of the Shack-Hartmann sensor is increased by rotational repositioning. Further it is shown that aberrations can be visualized by numerically subtracting the dominant low-order aberrations tip, tilt and defocus from individual subaperture recordings. Finally, section 5 concludes the paper and briefly outlines future work.

2. SCANNING SHACK-HARTMANN SENSOR

A Shack-Hartmann sensor (Figure 1) consists of a microlens array and an image sensor. Each microlens produces a focused spot on the image sensor, the position of the spot being dependent on the local slope of the wavefront incident on the microlens. This is illustrated in Figure 1 a). From the recorded spot pattern, local slopes can be calculated and then used to reconstruct the wavefront shape incident on the sensor [Platt and Shack (2001)]. Shack-Hartmann sensors offer a high measurement speed, are relatively robust to vibrations and have sub-wavelength resolution [Thier et al. (2013)].

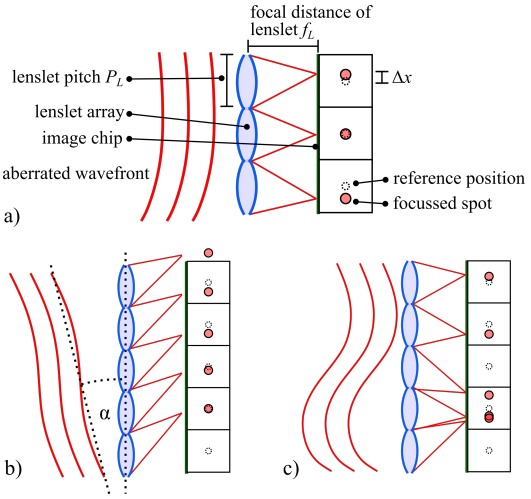

Fig. 1. The working principle of a Shack-Hartmann wavefront sensor. a) Each lenslet forms a focussed spot on the image sensor. The deviations of the spots from their reference positions can be identified. b) An angle α between wavefront and sensor causes the spots to leave their subapertures. c) High wavefront curvature leads to ambiguities in spot assignment.

The Shack-Hartmann sensor's dynamic range is limited by two wavefront characteristics: wavefront slope and wavefront curvature [Rocktäschel and Tiziani (2002)]. Wavefront slope describes the average angle between wavefront and sensor aperture. If this angle is too high, the lenslet array does not form spot images on the sensor chip (see Figure 1 b)). Spot deviation Δx can be related to incidence angle α and lenslet focal length with the relation

$$\Delta x = f_L \cdot \tan(\alpha) \tag{1}$$

(adapted from [Chernyshov et al. (2005)]). To ensure that spots are registered within their respective subapertures, this limits the maximum allowed incidence angle to

$$\alpha_{max} = \frac{P_L}{2 \cdot f_L} \tag{2}$$

(with lenslet pitch P_L as in Fig. 1 a)). For typical Shack-Hartmann sensor parameters ($P_l = 100 - 200\mu$m, $f_l = 3 -$ 10mm), α_{max} is only a few degrees (1-5°). Wavefront curvature describes the local variation of wavefront slope. If the curvature is too high, lenslets may form spots in the same position on the image chip, leading to ambiguities (see Figure 1 c)).

Figure 2 shows a schematic of a transmissive freeform lens. Instead of measuring the surface geometry of the lens, it is proposed to measure the resulting wavefront. This constitutes a measurement of part *performance* instead of part *surface*, thus evading the insecurities typically related to measuring surfaces in order to predict performance. The Shack-Hartmann sensor is limited by its finite aperture size

Post-print version of the article: M. E. Fuerst and G. Schitter, "Scanning Wavefront Sensor for Measurement of Highly Divergent Optics," *IFAC PapersOnLine*52-15 (2019) 25–30, 2019. DOI: 10.1016/j.ifacol.2019.11.644

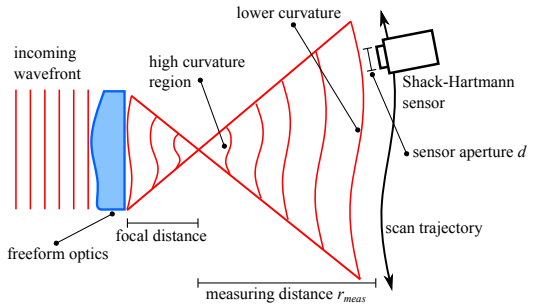

Fig. 2. The proposed measurement strategy for freeform optics utilizing a scanning wavefront sensor. The incoming, collimated light is shaped by the optics and the resulting wavefront is observed.

and its dynamic range considering maximum wavefront curvature. Both limitations could be overcome by the use of additional optical components to collimate and resize the wavefront. However, the added optical components have to be very specific and add additional aberrations and alignment problems [Fuerst et al. (2018)]. With a scanning setup, wavefront slope and curvature can be dealt with by increasing the measurement distance and repositioning the Shack-Hartmann sensor along the expected wavefront shape. Considering a spherical wave, the incidence angle α (comp. Fig. 1 b)) between Shack-Hartmann sensor and wavefront is related to the measurement distance r_{meas} (comp. Fig. 2))as

$$r_{meas} = \frac{d}{2 \cdot \sin \alpha} \tag{3}$$

with d being the diameter of the sensor aperture. It follows, that the angle α drastically decreases when the ratio $\frac{r_{meas}}{d}$ is increased:

$$\alpha = \arcsin \frac{d}{2 \cdot r_{meas}} \tag{4}$$

For typically acceptable incidence angles of below 5°, a measurement distance of at least 5 times the sensor aperture is required. To keep the incidence angle below 3°, the sensor is placed 10 times its aperture diameter from the spherical wave origin. Instead of *optical* insecurities, this adds *mechanical* insecurities that need to be evaluated for the system. Once these are known, the same measurement system can be used for a large range of optical parts without the need for any null-optics or reference shapes.

To fully scan the wavefront produced by a freeform lens, a 5-degrees-of-freedom positioning system is required. Position data and wavefront data is required to reconstruct the global wavefront. In case of rotational symmetry of the part (e.g. aspherical lenses), 3 degrees of freedom are sufficient as in that case, a scan along a single line crossing optical axis is sufficient. Therefore, a first experimental 3-DOF-system was constructed to investigate a rotationally symmetric lens, as described in the following section.

3. EXPERIMENTAL SETUP

To investigate the measurement capabilities of the 3-degrees-of-freedom scanning Shack-Hartmann setup, a rotationally symmetric, highly divergent wavefront is investigated. Such highly divergent wavefronts occur for instance in high-resolution microscopy or confocal displacement sensors. The lateral resolution of these applications is dictated by the numerical aperture (NA) of the lens or lens stack which is proportional to the divergence angle of the focussed beam. Since high numerical apertures are needed for small measuring spots, the resulting wavefront is highly curved and thus exceeds the dynamic range of a single, static Shack-Hartmann sensor. With the Scanning Shack-Hartmann Sensor (SSHS), these limitations can be overcome.

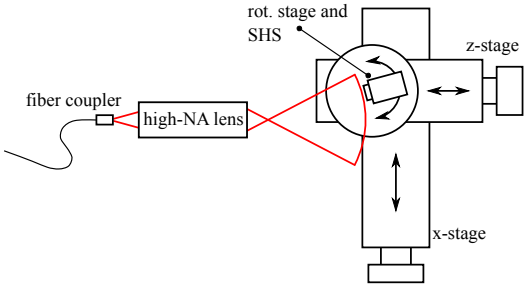

Fig. 3. Schematic view of the setup used to investigate the proposed measurement strategy for freeform optics by testing it on a high-NA optic. A laser diode is coupled to an optical fiber and the light exiting the fiber at a fiber coupler (FC) is used to illuminate a high-NA lens. The resulting, highly divergent wavefront is measured with the scanning Shack-Hartmann sensor.

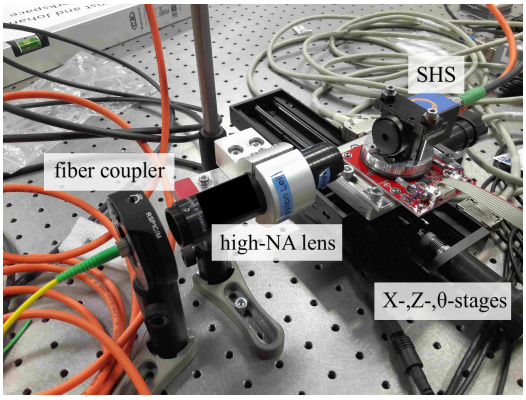

Fig. 4. The setup used for first investigations of the proposed measurement strategy. A 635 nm laser diode was coupled to a single-mode fiber to provide a monochromatic near-point light source for the high-NA lens. The Shack-Hartmann sensor is mounted on two motorized linear stages and one motorized rotary stage.

Figure 3 depicts the selected use case and the scanning setup. The setup consists of two motorized linear stages and one motorized rotary stage, meaning the Shack-Hartmann sensor can be positioned with 3 degrees of freedom (moving along a 2D-trajectory with arbitrary

Post-print version of the article: M. E. Fuerst and G. Schitter, "Scanning Wavefront Sensor for Measurement of Highly Divergent Optics," *IFAC PapersOnLine*52-15 (2019) 25–30, 2019. DOI: 10.1016/j.ifacol.2019.11.644

orientation). As this setup does not provide enough degrees of freedom to scan a fully freeform wavefront without any symmetries, a highly divergent, rotationally symmetric, wavefront was chosen as a test case. The linear stages (VT-80, PI Physik Instrumente, Braunschweig, Germany) provide a travel range of 200 mm and 50 mm, respectively, while their internal encoders have a resolution of 500 nm. The rotary stage (ELL-8M model from Thorlabs, USA) can be rotated by 360°, and offers an encoder resolution of 1.4 mdeg. A Shack-Hartmann sensor (model HR-2 from Optocraft, Erlangen, Germany) is used for the wavefront measurements. It has a rectangular aperture of 11.2 × 7 mm over which 85 × 53 lenslets with 130 μm pitch are distributed and its measurement rate is up to 18 Hz. Figure 4 shows the setup as assembled in the laboratory.

3.1 Experiments

With the constructed 3-degrees-of-freedom setup, the wavefront generated by a high-NA lens is investigated. A 635 nm laser diode was coupled to a single-mode optical fiber. The other end of the fiber was attached to a fiber coupler without collimating optics, thus serving as a monochromatic near-point light source for the high-NA lens.

A circular trajectory was chosen to scan the wavefront as that shape is close to the expected (ideal) shape of the investigated wavefront. Figure 5 illustrates the reasons for choosing a circular scanning trajectory and orienting the sensor tangentially to the wavefront: To scan a divergent wavefront, the sensor has to be moved from the optical axis of the optic under test. This position can be characterized by an angle α. For a linear scan trajectory, using a single, linear stage, the incidence angle β between wavefront and sensor aperture equals α, typically exceeding the dynamic range of a Shack-Hartmann sensor for angles of approximately $3 - 5°$. Addition of a rotational stage on which the sensor is mounted removes this limitation, as the stage angle θ can be adjusted to equal α, keeping β close to zero. In this case, however, the measurement distance would increase with α. To keep the measurement distance (distance between wave origin and sensor) constant, a second linear stage (Z-direction in Fig. 5) is added and a circular scan trajectory is chosen.

The radius of the scanning trajectory was chosen to be large enough that the wavefront curvature incident on the sensor is small enough to not exceed the dynamic range of the Shack-Hartmann sensor (compare Equation 4) and the spacing of the measurement positions was chosen so that the subapertures overlap. The Shack-Hartmann sensor was moved to 11 discrete positions spaced 3° apart in a distance of 54 mm to the focal point of the high-NA lens (the "origin" of a spherical wave). At each position, the Shack-Hartmann sensor is automatically pointed towards the expected position of the focal point and an image is recorded. For the presented experiments, this was done in a purely feed-forward controlled way and with coarse, manual alignment. As dicussed in the results section, the information collected by such a coarse run can be used to automatically improve the scanning trajectory for another measurement.

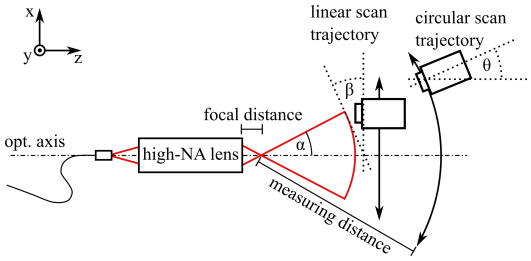

Fig. 5. Comparison of a linear and a circular scan trajectory. For sensor positions off the optical axis, an angle β between sensor and wavefront occurs. This can be negated by rotating the sensor by an angle θ. Note that $\alpha = \beta = \theta$.

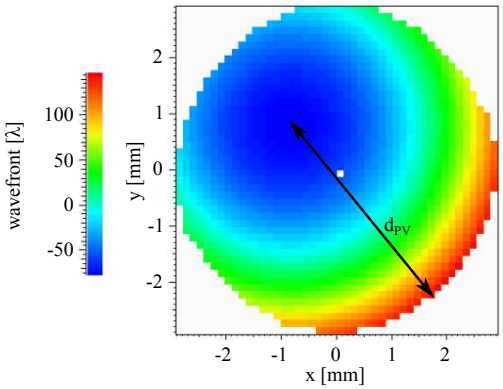

Fig. 6. An exemplary wavefront image from the measurement position -15°. The image is dominated by the low-order aberrations tip, tilt and defocus. The difference between the highest and the lowest point (peak-to-valley) is $PV = 225\lambda = 142$ μm and the distance between these two values is $d_{PV} = 4.044$ mm.

From the spot patterns, local wavefront gradients (slopes) are calculated and a 2D-polynomial function is fitted to match the observations (least-square-fit). Next, the wavefront shape is decomposed into Zernike base polynomials and their respective coefficients are calculated. Zernike polynomials are widely used in optics since they directly relate to basic optical aberrations such as tip, tilt, defocus, coma or astigmatism [Dai (2008)]. This is done to analyze the recorded wavefront images and also allows to numerically compensate for low-order aberrations.

4. RESULTS AND DISCUSSION

Figure 6 shows a single measured subaperture on the described trajectory. The imaged wavefront subaperture resembles part of a sphere, which is expected when measuring on a divergent wavefront. From the detected peak-to-valley variation of $PV = 225\lambda = 142$ μm and the measured distance from peak to valley $d_{PV} = 4.044$ mm, the radius R of the observed sphere can be calculated:

$$R = \frac{d_{PV}^2 + PV^2}{2 \cdot PV} = 57.66mm \qquad (5)$$

Post-print version of the article: M. E. Fuerst and G. Schitter, "Scanning Wavefront Sensor for Measurement of Highly Divergent Optics," *IFAC PapersOnLine*52-15 (2019) 25–30, 2019. DOI: 10.1016/j.ifacol.2019.11.644

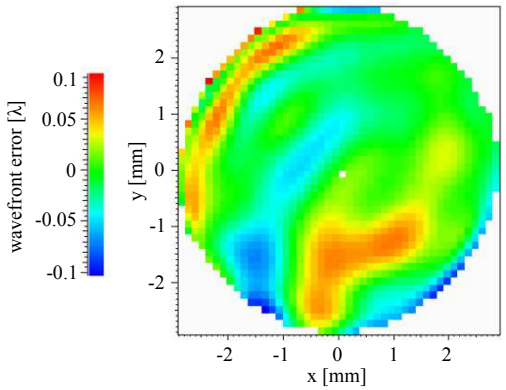

Fig. 7. A map of residual wavefront errors, when the low-order aberrations tip, tilt and defocus are subtracted from the recorded wavefront shown in Figure 6. All measurements were taken for a single wavelength (635 nm).

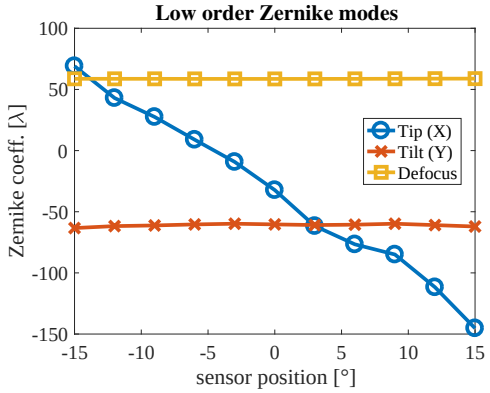

Fig. 8. Recorded low order Zernike coefficients via measurement position. The defocus- and tilt- (Y) coefficients are approximately constant while the tip (x) coefficient varies linearly. This can be explained by positioning errors.

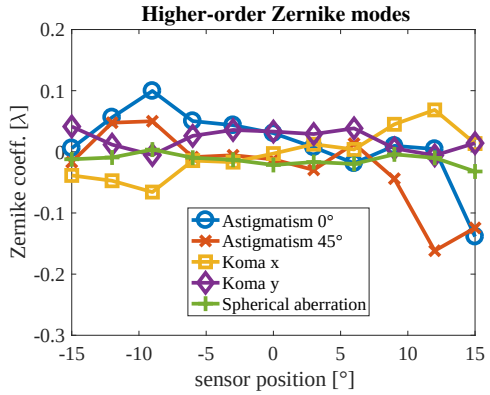

Fig. 9. The higher-order Zernike coefficients for astigmatism, coma and spherical aberration vary with the measurement position, but are relatively small in magnitude.

This is in agreement with the chosen measurement distance. Zernike analysis shows that the image is dominated by tip, tilt and defocus components. Defocus is responsible for the sphericity of the image while tip and tilt cause the visible shift of the center of the image. By subtracting these low-order aberration terms, the aberrations superimposed on the general sphere shape can visualized. This is shown in Figure 7, where only the residual wavefront error is visible. Peak-to-valley, this residual error is 0.2 λ for the presented subaperture, indicating a good quality lens.

Figure 8 compares the calculated low-order Zernike coefficients for each individual measurement position. These low order Zernike polynomials describe the wavefront tilt (X and Y) and defocus (deviation from the plane wave), as observed in the wavefront region incident on the sensor. Since a circular trajectory was chosen for the experiments and a divergent wavefront is under test, a constant defocus component is expected and can be observed (fig. 8, top line). The constant tilt (Y) coefficient can be explained by the scanning wavefront sensor and the optic under test not being set up at the exact same height from the optical table. This means that the optical axis of the high-NA lens is not in the same plane as the circular trajectory which is also visible in Figure 6. The linearly varying tilt (X) coefficient results from a mismatch of the center of the scanning trajectory and the focal point along the optical axis. As a next step, this could be automatically compensated by re-calculating the measurement positions and repeating the scanning measurement.

The presented low order aberrations result from geometrical mismatches and misalignments and can be identified as such. To evaluate the optical quality of the system under test, higher order aberrations need to be analyzed. This can be done by correcting each individual subaperture as shown exemplarily in Figure 7 and interpreting this set of images. Figure 9 presents the single-subaperture higher-order aberration coefficients over measurement position. It can be seen that these higher-order aberrations are consistently much smaller in magnitude than the low order aberrations but do increase towards the ends of the measurement range. However, since the coefficients are calculated for individual subapertures, they are not representative for the complete (global) wavefront (e.g. a coma aberration in a single subaperture does not indicate a coma aberration of the global wavefront). A more meaningful metric is the residual wavefront error, which is the peak-to-valley number of wavefront error when the low order aberrations are subtracted. This residual error is below 0.7 λ for all measured positions, providing a first estimate of the optical system's quality. For more valid measurements, the wavefront information of all subapertures needs to be combined with each other and the positioning data, which is part of ongoing work.

In summary, it is shown that the dynamic range limitations of the Shack-Hartmann sensor can be overcome by repositioning and tangential orientation of the Shack-Hartmann sensor to acquire wavefront images of subapertures that

Post-print version of the article: M. E. Fuerst and G. Schitter, "Scanning Wavefront Sensor for Measurement of Highly Divergent Optics," *IFAC PapersOnLine*52-15 (2019) 25–30, 2019. DOI: 10.1016/j.ifacol.2019.11.644

can be further processed to obtain the global wavefront information.

5. CONCLUSION

The Scanning Shack-Hartmann approach offers a versatile, flexible way to measure freeform optics with reasonable measurement accuracy and measurement times. A first automatic setup is proposed and demonstrated to show the feasibility of the concept by taking measurements on a highly divergent wavefront. It is shown that the dynamic range of the Shack-Hartmann sensor can be increased by repositioning the sensor with respect to the wavefront. Future investigation is focussed on the tradeoffs between measurement speed, positioning accuracy, and measurement resolution. Next steps will be automatic correction of misalignments and evaluation of the global wavefront shape. For this purpose, stitching algorithms [Chen et al. (2017)], that incorporate both the measurement data and the position data, have to be developed.

ACKNOWLEDGEMENTS

The financial support by the Christian Doppler Research Association, the Austrian Federal Ministry for Digital and Economic Affairs, and the National Foundation for Research, Technology and Development, as well as MICRO-EPSILON MESSTECHNIK GmbH & Co. KG and ATENSOR Engineering and Technology Systems GmbH is gratefully acknowledged.

REFERENCES

Assefa, B.G., Pekkarinen, M., Saastamoinen, T., Biskop, J., Kuittinen, M., Turunen, J., and Saarinen, J. (2018). Design and characterization of 3D-printed freeform lenses for random illuminations. *Light-Emitting Diodes: Materials, Devices, and Applications for Solid State Lighting XXII*, (February), 53. doi:10.1117/12.2288223.

Burada, D.R., Pant, K.K., Bichra, M., Khan, G.S., Sinzinger, S., and Shakher, C. (2017). Experimental investigations on characterization of freeform wavefront using Shack–Hartmann sensor. *Optical Engineering*, 56(08), 1. doi:10.1117/1.OE.56.8.084107.

Chen, S., Xue, S., Wang, G., and Tian, Y. (2017). Subaperture stitching algorithms: A comparison. *Optics Communications*, 390(January), 61–71. doi: 10.1016/j.optcom.2016.12.067.

Chernyshov, A., Sterr, U., Riehle, F., Helmcke, J., and Pfund, J. (2005). Calibration of a Shack-Hartmann sensor for absolute measurements of wavefronts. *Applied Optics*, 44(30), 6419–6425. doi:10.1364/AO.44.006419.

Dai, G.M. (2008). *Wavefront optics for vision correction Vol. 179*. Bellingham: SPIE press.

Fang, F.Z., Zhang, X.D., Weckenmann, A., Zhang, G.X., and Evans, C. (2013). Manufacturing and measurement of freeform optics. *CIRP Annals - Manufacturing Technology*, 62(2), 823–846. doi:10.1016/j.cirp.2013.05.003.

Fuerst, M., Unger, S., Ito, S., and Schitter, G. (2018). Wavefront measurement based feedback control for automatic alignment of a high-NA optical system. *Journal of Physics: Conference Series*, 1065, 32001. doi: 10.1088/1742-6596/1065/3/032001.

Graves, L.R., Smith, G.A., Apai, D., and Kim, D.W. (2019). Precision Optics Manufacturing and Control for Next - Generation Large Telescopes. *Nanomanufacturing and Metrology*, (0123456789). doi:10.1007/s41871-019-00038-2. URL `https://doi.org/10.1007/s41871-019-00038-2`.

Henselmans, R., Cacace, L.A., Kramer, G.F.Y., Rosielle, P.C.J.N., and Steinbuch, M. (2011). The NANOMEFOS non-contact measurement machine for freeform optics. *Precision Engineering*, 35(4), 607–624. doi: 10.1016/j.precisioneng.2011.04.004.

Kim, B.C., Saiag, T., Wang, Q., Soons, J., Polvani, R.S., and Griesmann, U. (2004). The Geometry Measuring Machine (GEMM) Project at NIST. *Proceedings of the 2004 ASPE Winter Top. Meeting, North Carolina, USA*, 3–6.

Li, Q. and Fang, F. (2019). Advances and challenges of soft contact lens design for myopia control. *Applied Optics*, 58(7), 1639. doi:10.1364/AO.58.001639.

Pant, K.K., Burada, D.R., Bichra, M., Singh, M.P., Ghosh, A., Khan, G.S., Sinzinger, S., and Shakher, C. (2015). Subaperture stitching for measurement of freeform wavefront. *Applied Optics*, 54(34), 10022. doi: 10.1364/AO.54.010022.

Platt, B.C. and Shack, R. (2001). History and Principles of Shack-Hartmann Wavefront Sensing. *Journal of Refractive Surgery*, 17(5), S573–S577. doi:10.3928/1081-597x-20010901-13.

Reimers, J., Bauer, A., Thompson, K.P., and Rolland, J.P. (2017). Freeform spectrometer enabling increased compactness. *Light: Science & Applications*, 6(7), e17026. doi:10.1038/lsa.2017.26.

Rocktäschel, M. and Tiziani, H.J. (2002). Limitations of the Shack-Hartmann sensor for testing optical aspherics. *Optics and Laser Technology*, 34(8), 631–637. doi: 10.1016/S0030-3992(02)00069-5.

Savio, E., De Chiffre, L., and Schmitt, R. (2007). Metrology of freeform shaped parts. *CIRP Annals - Manufacturing Technology*, 56(2), 810–835. doi: 10.1016/j.cirp.2007.10.008.

Thier, M., Paris, R., Thurner, T., and Schitter, G. (2013). Low-latency shack-hartmann wavefront sensor based on an industrial smart camera. *IEEE Transactions on Instrumentation and Measurement*, 62(5), 1241–1249. doi:10.1109/TIM.2012.2223333.

Zapico, P., Patiño, H., Valiño, G., Fernández, P., and Rico, J.C. (2018). CNC centralized control for digitizing freeform surfaces by means of a conoscopic holography sensor integrated in a machining centre. *Precision Engineering*, 55(November 2018), 474–483. doi: 10.1016/j.precisioneng.2018.11.001.